Journal of Materials Chemistry C

Efficient near-infrared (NIR) polymer light-emitting diodes (PLEDs) based on heteroleptic Iridium(III) complexes with post-modification effect of intramolecular hydrogen bond or BF2-chelation

Journal:	*Journal of Materials Chemistry C*
Manuscript ID	TC-REV-07-2018-003432.R1
Article Type:	Paper
Date Submitted by the Author:	27-Aug-2018

Complete List of Authors:	Fu, Guorui; Northwest University Zheng, Hao; Northwest University Hui, Yani; Northwest University Li, Wentao; Northwest University Lv, Xingqiang; Northwest University, ; Hong Kong Baptist University, Department of Chemistry He, Hongshan; Eastern Illinois University, Chemistry

Journal Name

ARTICLE

Efficient near-infrared (NIR) polymer light-emitting diodes (PLEDs) based on heteroleptic Iridium(III) complexes with post-modification effect of intramolecular hydrogen bond or BF_2-chelation

Received 00th January 20xx,
Accepted 00th January 20xx

DOI: 10.1039/x0xx00000x

www.rsc.org/

Guorui Fu,[a] Hao Zheng,[a] Yani He,[a] Wentao Li,[a] Xingqiang Lü[a,*] and Hongshan He[b,*]

As to heteroleptic iridium(III)-complex capable of near-infrared (NIR) emitting, the elaboration of ancillary ligand is unexplored enough. In this study, through the OH-modification at the 3-position of picolinato (pic) ancillary ligand, we report two new complexes **[Ir(iqbt)$_2$(hpa)]** (**1**; **Hqibt** = 1-(benzo[*b*]-thiophen-2-yl)-isoquinoline; **hpa** = 3-hydroxypicolinate) with intramolecular hydrogen bond and **[Ir(iqbt)$_2$(BF$_2$-hpa)]** (**2**) by further BF_2-chelation, exhibiting the desirable NIR luminescent properties (λ_{em} = 700 nm with a shoulder at 760 nm, lifetime τ = 2.13 μs and quantum yield Φ_{PL} = 0.13 for **1** versus λ_{em} = 692 nm with a shoulder at 756 nm, lifetime τ = 0.76 μs and quantum yield Φ_{PL} = 0.08 for **2**) in the respective solution at RT. Moreover, two series of solution-processed NIR polymer light-emitting diodes (PLEDs-I-II) are fabricated from these two complexes in the presence of TmPyPB-assisted (TmPYPB = 1,3,5-tri[(3-pyridyl)-phen-3-yl]benzene) carrier balance or not, respectively, where superior performance (η_{EQE}^{max} = 2.22% and almost negligible efficiency-roll-off) is obtained for complex-**1**-doping NIR-PLED-II especially with the facilitated electron-transport.

1. Introduction

Iridium(III)-complex-based lumophores are of particular interest on organic light-emitting diodes (OLEDs),[1] apart from their potential applications in light-emitting electrochemical cells,[2] photo-catalysis,[3] sensing[4] and biolabeling,[5] which should be due to iridium(III)-induced strong spin-orbit coupling capable of harvesting of both singlet and triplet excitons. However, contrasted to the concerted efforts to monochromatic (blue, green, yellow, orange or red)[6] and panchromatic (white-light)[7] OLEDs that covered the whole visible electromagnetic spectrum range, near-infrared (NIR) electroluminescent (EL) devices based on iridium(III)-complex phosphors are much underperformed.[8] Convincingly, this category of emitters suffers from an intrinsic obstacle of unsatisfactory NIR quantum efficiency since luminescent quantum yields tend to decrease with an increasing emission wavelength in accordance with the energy gap law.[9] Nonetheless, driven by emergent needs[10] of NIR-OLEDs for military photonic devices, night-version readable displays and telecommunications, promising NIR-emissive materials[11] included iridium(III)-complex emitters are currently under investigation.

As a matter of fact, to the best of our knowledge, although the state-of-art NIR-OLEDs were still focalized on Pt(II)-complex phosphors,[12] their detrimental efficiency-roll-off arisen from the facile aggregation of the square-planar systems impeded the option's future popularity. By contrast, iridium(III)-complex-counterparts[8, 11d] with typical octahedral configuration and rather short triplet lifetime should be ideal candidates for NIR-dye-resources, and the realization of desirable high-efficiency while significantly alleviated efficiency-roll-off as compensation for their NIR-OLEDs is much attracting.[13, 14] From the viewpoint of lowering the emission energy of iridium(III)-complexes into a restrictive NIR regime (700-2500 nm), the most successful approach is focused on the π-conjugation expansion of the C^N-cyclometalated main ligand especially incorporated with electron-rich substituents to afford the expected homoleptic ([Ir(C^N)$_3$]) for NIR-OLEDs[13] or heteroleptic ([Ir(C^N)$_2$(L^X)]) for NIR-OLEDs[14] or NIR-PLEDs,[15] respectively. Considering the venture of aggregation-induced quenching effect[16] from large π-conjugation of the C^N main ligand, the modification

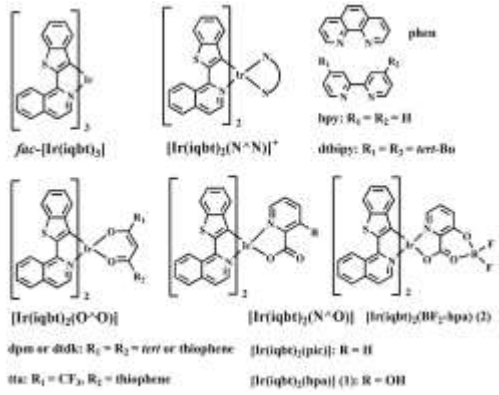

Scheme 1. Structural scheme for typical heteroleptic [Ir(iqbt)$_2$(L^X)] complexes versus the homoleptic *fac*-[Ir(iqbt)$_3$] complex.

[a]*School of Chemical Engineering, Shaanxi Key Laboratory of Degradable Medical Material, Northwest University, Xi'an 710069, Shaanxi, China.*
[b]*School of Chemistry, Eastern Illinois University, Charleston, IL 61920, USA*
**E-mail: lvxq@nwu.edu.cn; hhe@eiu.edu; Tex/Fax: +86-29-88302312*
Electronic Supplementary Information (ESI) available: [Starting materials and characterization; XRD; NMR, UV, PL]. See DOI: 10.1039/x0xx00000x

of the L^X ancillary ligand[17] can be used to effectively narrow the energy gap as an alternative, while it does not take effect as a universal. For example, starting from the parent complex *fac*-[Ir(iqbt)$_3$] (Scheme 1) doped into PVK-PBD (PVK = poly(*N*-vinylcarbazole); PBD = 2-(4-biphenyl)-5-(4-*tert*-butyl-phenyl)-1,3,4-oxadiazole) host, whose deep-red-light PLED emitted at 690 nm with a good efficiency (η_{EQE} (external quantum efficiency) of 1.4%),[18] significant electronic perturbation could be approached by introducing one β-diketonate ancillary ligand (O^O) to obtain heteroleptic Ir(III)-complexes ([Ir(iqbt)$_2$(O^O)], O^O = Hdpm, Htta or Hdtdk also Scheme 1).[17b] Through the decreases of their both E_{HOMO} (-5.31 ~ -5.15 eV) and E_{LUMO} (-2.96 ~ -2.71 eV) energy levels as compared to those (-5.00 and -2.11 eV) of *fac*-[Ir(iqbt)$_3$], the narrowed energy gaps (2.34-2.35 eV) induced desirable bathochromatic shifts (14-20 nm) into the NIR region (λ_{em} = 704-710 nm), and their PVK-OXD7-matrixed (OXD7 = 1,3-bis(5-(4-*tert*-butyl-phenyl)-1,3,4-oxadiazol-2-yl)benzene) PLEDs were realized with a considerable η_{EQE} of 3.07% at 714 nm. However, based on an N^N (phen, bpy or dtbipy) or N^O (pic) ancillary ligand (also in Scheme 1) instead,[17a] the lower energy gap (2.938 eV) for [Ir(iqbt)$_2$(pic)] than those (3.068-3.072 eV) for [Ir(iqbt)$_2$(N^N)]$^+$ was consistent with the slight red-shift at 698 nm while slight blue-shifts at 682-683 nm in relative to that (690 nm) of *fac*-[Ir(iqbt)$_3$]. On one hand, the unconventional bathochromatic shift caused by pic ancillary ligand is significantly contrary to the rational blue-shift for well-known FIrpic (FIrpic = bis[2-(4,6-difluorophenyl)pyridinato-C^2,N](pic)-iridium(III)),[19] while endows an opportunity to the emissive wavelength into the true NIR regime. More importantly, modification[20] of pic-derived ancillary ligands especially at the chemically reactive 3- or 4-position can resolve the problem to insoluble [Ir(iqbt)$_2$(pic)] for solution-processed OLEDs. Herein, in light of the 3-position modification of a simple hydroxyl group[20c, 20e] or four-coordinate organoboron moiety[21] into pic capable of smooth color-tuning within the visible range, two new Ir(III)-complexes of **[Ir(iqbt)$_2$(hpa)]** (**1**) and **[Ir(iqbt)$_2$(BF$_2$-hpa)]** (**2**) (also in Scheme 1) are rationally designed by introducing one of specific pic-derived ancillary ligands at the chemically reactive 3-position. And through the effect of intramolecular hydrogen bond or BF$_2$-chelation involved, their significantly red-shifted emissions into NIR regime suitable for solution-processing NIR-PLEDs are also expected.

2. Experimental section

The information of starting materials and general characterization methods has been depicted in Electronic Supplementary Information (ESI). The C^N main ligand **Hiqbt** was synthesized from the improved coupling reaction of 2-Cl-isoquinoline while not 2-Br-isoquinoline with benzo[*b*]thien-2-y boronic acid as the literature.[18] The synthesis of the μ-chloro-bridged dimmer intermediate **[Ir(iqbt)$_2$(μ-Cl)]$_2$** was according to a well-established procedure from the literature.[17]

Synthesis of complex [Ir(iqbt)$_2$(hpa)] (1)

To a solution of the μ-chloro-bridged dimmer intermediate **[Ir(iqbt)$_2$(μ-Cl)]$_2$** (270 mg, 0.18 mmol) in 2-ethoxyethanol (10 mL), 3-hydroxy-picolinic acid (**Hhpa**, 75 mg, 0.54 mmol) and anhydrous Na_2CO_3 (190 mg, 1.8 mmol) were added, and the reaction mixture was heated to reflux under a dry N_2 atmosphere for 24 h. After cooling to room temperature, the saturated brine (30 mL) was added, and the resulting suspension was filtered. Then the crude solid product was purified with column chromatography on silica gel with ethyl acetate/petroleum ether (v/v = 3:1) as the eluent. Recrystallization from CH_2Cl_2/ethyl acetate (EAC) gives a brown-red microcrystalline product as desired. Yield: 46 mg (30%). Calc. for $C_{40}H_{24}N_3O_3S_2Ir$: C, 56.46; H, 2.84; N, 4.94%. Found: C, 56.41; H, 2.92; N, 4.92%. FT-IR (KBr, cm^{-1}): 3401 (b), 2956 (m), 2923 (m), 2849 (m), 1727 (w), 1644 (w), 1597 (w), 1546 (w), 1503 (w), 1456 (4), 1440 (m), 1427 (m), 1378 (w), 1342 (w), 1308 (w), 1258 (m), 1023 (vs), 800 (s), 746 (m), 728 (w), 708 (w), 689 (m), 667 (w), 617 (w), 596 (w), 582 (w), 568 (w), 551 (w), 518 (w). ^{1}H NMR ($CDCl_3$, 400 MHz): δ (ppm) 12.91 (s, 1H, -OH), 9.24 (d, 1H, -Ph), 9.00 (d, 1H, -Ph), 8.45 (d, 1H, -Ph), 8.01 (d, 1H, -Ph), 7.80 (m, 7H, -Ph), 7.40 (m, 6H, -Ph), 7.22 (m, 1H, -Ph), 7.07 (t, 1H, -Ph), 6.99 (d, 1H, -Ph), 6.87 (d, 1H, -Ph), 6.68 (d, 1H, -Ph), 6.60 (d, 1H, -Ph). ESI-MS (in CH_2Cl_2) *m*/*z*: 852.10 (100%), [M+H]$^+$; 713.07 (16%), [M-(hpa)]$^+$.

Synthesis of complex [Ir(iqbt)$_2$(BF$_2$-hpa)] (2)

To a solution of the obtained **[Ir(iqbt)$_2$(hpa)]** (150 mg, 0.13 mmol) in dry CH_2Cl_2 (10 mL), boron trifluoride-diethyl etherate (220 μL, 1.3 mmol) was added, and the resultant mixture was stirred at room temperature under an N_2 atmosphere for 24 h. The solvent was removed under reduced pressure. The residual was dissolved in absolute CH_2Cl_2 and further purified by flash-column chromatography on silica gel using EAC/petroleum ether (v/v = 1:1.2) as the eluent, giving a brown-red microcrystalline solid. Yield: 60 mg (51%). Calc. for $C_{40}H_{23}N_3O_3S_2BF_2Ir$: C, 53.45; H, 2.58; N, 4.68%. Found: C, 53.32; H, 2.63; N, 4.62%. FT-IR (KBr, cm^{-1}): 3052 (w), 2954 (w), 2925 (w), 2853 (w), 2024 (w), 1730 (w), 1624 (s), 1591 (w), 1573 (w), 1544 (w), 1494 (m), 1454 (s), 1439 (s), 1425 (s), 1381 (w), 1368 (w), 1341 (m), 1310 (m), 1281 (m), 1252 (w), 1234 (m), 1202 (m), 1152 (s), 1145 (m), 1133 (s), 1076 (m), 1054 (m), 1038 (vs), 953 (m), 916 (m), 848 (m), 810 (m), 764 (m), 741 (m), 729 (s), 707 (m), 689 (m), 675 (w), 661 (m), 640 (w), 620 (w), 603 (w), 566 (w), 528 (w). ^{1}H NMR ($CDCl_3$, 400 MHz): δ (ppm) 9.12 (d, 1H, -Ph), 9.03 (d, 1H, -Ph), 8.38 (d, 1H. Ph), 8.00 (d, 1H, -Ph), 7.95 (d, 1H, -Ph), 7.87 (m, 6H, -Ph), 7.78 (d, 1H, -Ph), 7.51 (q, 2H, -Ph), 7.39 (q, 1H, Ph), 7.31 (s, 2H, -Ph), 7.23 (t, 1H, -Ph), 7.14 (t, 1H, -Ph), 6.82 (q, 1H, -Ph), 6.69 (q, 1H, -Ph), 6.42 (d, 1H, -Ph), 6.08 (d, 1H, -Ph). ^{19}F NMR (100 MHz, $CDCl_3$-$CFCl_3$): δ (ppm) -142.9 ~ -143.0 (m, 2F, -BF$_2$). ESI-MS (in CH_2Cl_2) *m*/*z*: 900.09 (100%), [M+H]$^+$; 713.08 (23%), [M-(BF$_2$-hpa)]$^+$.

Computational study

Density functional theory (DFT) calculations were performed using a computational package under the B3LYP level[22] known to provide good fit to the geometric parameters. Ground state and triplet state geometries were optimized first in the semi-empirical PM3 mode then at the full DFT theory. "Double-ξ" quality basis sets were used for C, H, N and O (6-31G*) and Ir (LANL2DZ). An effective core potential (ECP) replaces the inner core electrons of Ir leaving the outer core [(5s)^2(5p)^6] electrons and the (5d)^6 valence electrons of Ir(III). All calculations were carried out with the Gaussian 03 software package using spin-restricted formalism.[23] Electron density diagrams of molecular orbitals were obtained with the ChemBioOffice 2010 software.

Structural design of NIR-PLEDs based on complex 1 or 2

Using the mixture of the guest Ir(III)-complex (**1** or **2**; 5 wt%) and the host PVK-OXD7 (2:1 of mass ratio) as the emissive layer, two series of NIR-PLEDs-I-II were fabricated by spin-coating with the

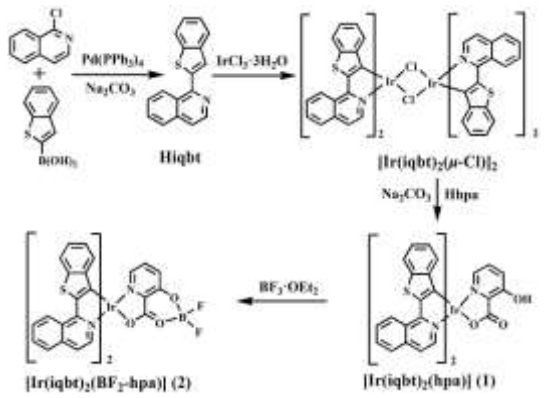

Scheme 2. Reaction scheme for the synthesis of the complexes [Ir(iqbt)$_2$(hpa)] (**1**) and [Ir(iqbt)$_2$(BF$_2$-hpa)] (**2**)

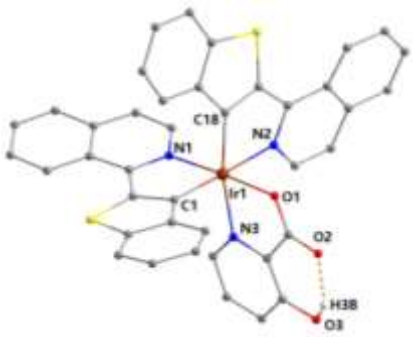

Figure 1. Perspective drawing of the mononuclear framework with the intra-molecular O3-H3B···O2 hydrogen bonding in complex **1**·$CH_3COOCH_2CH_3$; H atoms and the solvate $CH_3COOCH_2CH_3$ were omitted for clarity.

device configurations of ITO/PEDOT:PSS (40 nm)/PVK:OXD7:Ir(III)-complex (120 nm)/LiF (1 nm)/Al (100 nm) for NIR-PLEDs-I and ITO/PEDOT:PSS (40 nm)/PVK:OXD7:Ir(III)-complex (120 nm)/TmPyPB (15 nm)/LiF (1 nm)/Al (100 nm) for NIR-PLED-II, respectively. Among these materials, ITO (Indium tin oxide) was the coated glass substrate, and PEDOT:PSS (poly(3,4-ethylenedioxythiophene):poly(styrenesulfonate)) acts as the hole-injecting material. TmPyPB (1,3,5-tri[(3-pyridyl)-phen-3-yl]benzene) was used to further promote electron-transport ability in NIR-PLED-II. Details of the two series of PLEDs' fabrication and testing were presented in the ESI.

3. Results and discussion

Synthesis and characterization of complexes [Ir(iqbt)$_2$(hpa)] (1) and [Ir(iqbt)$_2$(BF$_2$-hpa)] (2)

The C^N main ligand **Hiqbt** was synthesized from the Suzuki coupling reaction[18] of cost-effective 2-Cl-isoquinoline with benzo[*b*]thien-2-y boronic acid in a yield of 73%. As shown in Scheme 2, reaction of **Hhpa** and the μ-chloro-bridged dimmer intermediate **[Ir(iqbt)$_2$(μ-Cl)]$_2$** rationally prepared from reaction of $IrCl_3 \cdot 3H_2O$ with the ligand **Hiqbt**,[17] gave rise to the desired product of complex **[Ir(iqbt)$_2$(hpa)]** (**1**). Further through the treatment of complex **[Ir(iqbt)$_2$(hpa)]** (**1**) with excess boron trifluoride-diethyl etherate, BF$_2$-chelated complex **[Ir(iqbt)$_2$(BF$_2$-hpa)]** (**2**) was obtained in a desirable yield (51%).

The two Ir(III)-complexes **1**-**2** soluble in common organic solvents were well-characterized by EA, FT-IR, NMR and ESI-MS. In their FT-IR spectra, contrasted to the band-like absorption at 3401 cm^{-1} assigned to the ν(OH-phenolic) vibration for complex **1**, its disappearance together with the additional ν(B-F)-vibrated strong absorption at 729 cm^{-1} elucidates the incorporation of BF$_2$-moiety in complex **2**. As to the ^{1}H NMR spectrum (Figure 1S) of complex **1**, the singlet proton resonance at δ = 12.91 ppm should ascribe to the formation of intra-molecular resonance-assisted hydrogen bond (RAHB, O-H···O). Through BF$_2$-chelation for complex **2**, the typical RAHB proton resonance disappears, and a relatively spread shift (δ from 9.12 to 6.08 ppm; also in Figure 1S) of the combined proton resonances of both (**iqbt**)$^-$ and (**hpa**)$^-$ ligands relative to that (δ = 9.24 to 6.60 ppm) of complex **1** is also observed. Moreover, the characteristic F signals at δ = -142.9 ~ -143.0 ppm in the ^{19}F NMR spectrum of complex **2** further confirm its successful BF$_2$-chelation.

Molecular structure of complex **1** was obtained by single-crystal X-ray diffraction analysis with crystallographic data in Tables 1 and 1S. Complex **1**·$CH_3COOCH_2CH_3$ crystallizes the monoclinic space group of *P2(1)/n*, and its asymmetry unit is composed of one mononuclear molecule **[Ir(iqbt)$_2$(hpa)]** (**1**) and one solvate $CH_3COOCH_2CH_3$. As shown in Figure 1, for the mononuclear host framework, two (**iqbt**)$^-$ main ligands with the similar C^N-chelated mode (C1^N1 and C18^N2) and one (**hpa**)$^-$ ancillary ligand with the N^O-chelated mode (N3^O1) coordinate to one Ir(III)-centered ion (Ir1) in a distorted octahedral coordination geometry, exhibiting the character of typical heteroleptic [Ir(C^N)$_2$(N^O)] complexes.[20] The *trans*-N and *cis*-metalated C atoms arrayed from the two (**iqbt**)$^-$ main ligands reveal the absence of symmetry in the [Ir(C^N)$_2$(N^O)] unit, which together with the formation of strong intra-molecular O3-H3B···O2 hydrogen-bond (2.568(6) Å and 147.2(3)°)[20c] are identical with the ^{1}H NMR analysis (Figure 1S) of complex **1**. The solvate of **1**·$CH_3COOCH_2CH_3$ within is not bounded to host framework and there has no observed interactions between. Furthermore, the ESI-MS spectra of the two Ir(III)-complexes **1**-**2**

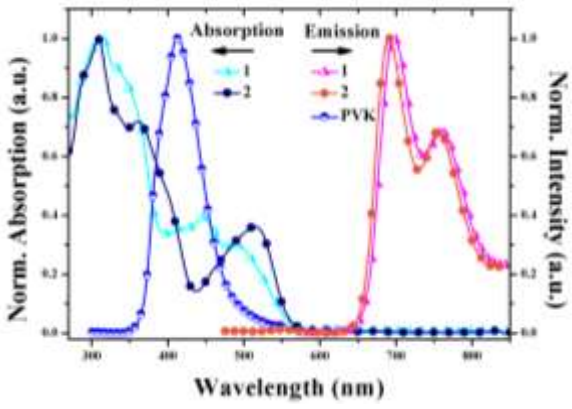

Figure 2. Normalized UV-Visible-NIR absorption and photoluminescence spectra for complexes **1**-**2** in degassed CH_2Cl_2 solution and PVK in solid film at RT.

Table 1 Photophysical and electrochemical properties of complexes **1**-**2** in solution at RT or 77 K

Complex	Absorption		Emission at 298 K				Emission at 77 K		Energy level	
	λ_{abs}[a]	λ_{em}[a]	τ	Φ_{em}[a]	k_r[a]	k_{nr}[a]	λ_{em}	τ	HOMO[b,c]	LUMO[b,c]
	(nm)	(nm)	(μs)		($\times10^5$ s^{-1})	($\times10^5$ s^{-1})	(nm)	(μs)	(eV)	(eV)
[Ir(iqbt)$_2$(hpa)] (1)	314, 420, 448, 492, 672	700, 760(sh)	2.13	0.13	0.61	4.08	704, 764(sh)	3.82	-5.47(-4.95)	-3.30(-2.12)
[Ir(iqbt)$_2$(BF$_2$-hpa) (2)]	308, 362, 402, 514, 670	692, 756(sh)	0.76	0.08	1.06	12.10	696, 755(sh)	1.89	-5.38(-5.19)	-3.19(-2.33)

[a] In degassed CH_2Cl_2 solution; Rate constant k_r and k_{nr} are calculated using the equations $k_r = \Phi_{em}/\tau$ and $k_{nr} = (1-\Phi_{em})/\tau$ on the assumption that $\Phi_{isc} = 1$ (ISC = intersystem crossing); [b,c] HOMO and LUMO levels are obtained from electrochemical determination and theoretic calculation, respectively.

exhibit a strongest mass peak at *m/z* 852.10 (**1**) or 900.09 (**2**) assigned to the major species $[M+H]^+$, respectively, indicating that the respective heteroleptic unit of complex **1** or **2** keeps stable in solution. The thermal properties of the two complexes **1**-**2** were investigated by thermogravimetric analysis (TGA), where as shown in Figure 2S, their decomposition temperatures (T_d, corresponding to 5% weight loss) are observed at 344 °C for complex **1** and 297 °C for complex **2**, respectively, indicative of their favourable thermal stability.

Photophysical properties of complexes [Ir(iqbt)$_2$(hpa)] (1) and [Ir(iqbt)$_2$(BF$_2$-hpa)] (2)

Photophysical properties of the C^N ligand **Hiqbt**, the N^O ancillary ligands **Hhpa** and **BF$_2$-hpa** and their two Ir(III)-complexes **1**-**2** in solution were measured using UV-visible absorption and photoluminescence (PL) spectrometers at room temperature or 77 K, and the results are summarized in Table 1 and Figures 2 and 3-5S. In comparison to the strong absorption bands limited in the $\lambda < 400$ nm range (Figure 3S) for the ligands **Hiqbt**, **Hhpa** and **BF$_2$-hpa**, both complexes **1**-**2** show the significantly broaden UV-Visible-NIR absorption spectra (Figure 2): intense absorption bands below 450 nm from the intra-ligand π-π* transitions, moderate bands in the range λ = 450-600 nm probably belonging to the mixed ^{3}LC/^{1,3}MLCT (LC = ligand-centered; MLCT = metal-to-ligand charge transfer, d-π*) transitions[17b] and even weak bands (672 nm for **1** or 670 nm for **2** shown in Table 1 and Figure 3S) extending over 600 nm from ground-state excitation into the lowest triplet state ($S_0 \rightarrow T_1$), respectively. Worthy of notice, the low-energy LC/MLCT band at 492 nm in complex **[Ir(iqbt)$_2$(hpa)]** (**1**) with intra-molecular hydrogen bond or at 514 nm in complex **[Ir(iqbt)$_2$(BF$_2$-hpa)]** (**2**) containing BF_2-moiety, is distinctively blue-shifted by 33-11 nm in relative to that (525 nm) of the parent complex [Ir(iqbt)$_2$(pic)],[17a] which should be resulted from the change of ancillary-ligand field strength. Moreover, in dependence of the intra-molecular hydrogen bonding or BF_2-chelation, the Ir(III)-centered d-(t_{2g}) orbital energy for complexes **1**-**2** is definitely controlled from the further OH- or BF_2-modification of the ancillary ligand.

Also as shown in Figure 2, upon photo-excitation (λ_{ex} = 544 nm, Figure 4S), complex **1** displays a typical NIR phosphorescence emission with a strong peak at 700 nm and a shoulder peak at 760 nm. By contrast, the strong emission peak (692 nm) of complex **2** lies at the edge of the NIR regime besides a shoulder around 756 nm at λ_{ex} = 539 nm (Figure 4S). As a result of the non-emissive character (Figure 5S) of both the C^N **Hiqbt** ligand and the N^O **Hhpa** or **BF$_2$-hpa** ancillary ligand in that NIR range, the NIR emissions of complexes **1**-**2** should originate from the ligands-perturbed ^{3}MLCT-excited state.[17b] Further as illustrated for the emission spectra (also in Figure 5S) of the two complexes **1**-**2** at 77 K, the 0-0 band appears at 704 nm for complex **1** or 696 nm for complex **2** with small bathochromatic shifts of about 4 nm compared to the RT spectra (Figure 2), confirming again the ^{3}MLCT character of the excited state. The emissive efficiency (Φ_{PL} = 0.13) of complex **1** in solution at RT comparable to that (Φ_{PL} = 0.12) of complex [Ir(iqbt)$_2$(pic)][17a] is much higher than that (Φ_{PL} = 0.08) of complex **2**. Interestingly, the emission lifetime (τ = 2.13 μs) of complex **1** is remarkably longer than that (τ = 0.76 μs) of complex **2** and those (τ = 0.72-1.44 μs) of complexes [Ir(iqbt)(O^O)][17b] at RT. This observation together with the substantial τ = 3.82 μs for **hpa**-related complex **1** at 77 K, should be attributed to the formation of intramolecular O-H···O hydrogen bond for a restrictive vibrational motion of the excited-state.[20c] Moreover, despite the desirably high radiative rate constants (k_r; 0.61×10^5 s^{-1} for **1** and 1.06×10^5 s^{-1} for **2**) of the two Ir(III)-complexes, the nonradiative rate (k_{nr}; 12.10×10^5 s^{-1}) for complex **2** is three times larger than that (4.08×10^5 s^{-1}) of complex **1**.

Electronic structure calculation and determination of the two Ir(III)-complexes 1-2

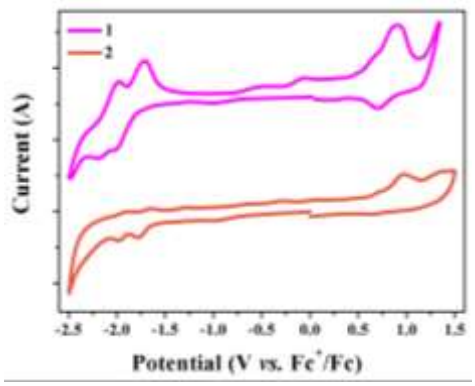

Figure 3. Cyclic voltammograms of complexes **1**-**2** recorded versus Fc^+/Fc in solution at RT under a N_2 atmosphere (scan rate = 100 mV/s).

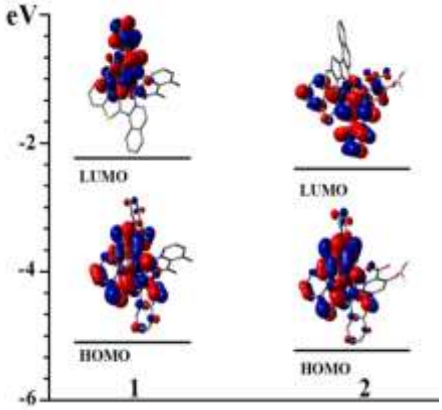

Figure 4. Optimized output geometry and frontier orbital diagrams for the Ir(III)-complexes **1**-**2** obtained from DFT calculations, where HOMO and LUMO refer to the highest occupied molecular orbital and the lowest unoccupied molecular orbital, respectively. All hydrogen atoms are omitted for clarity

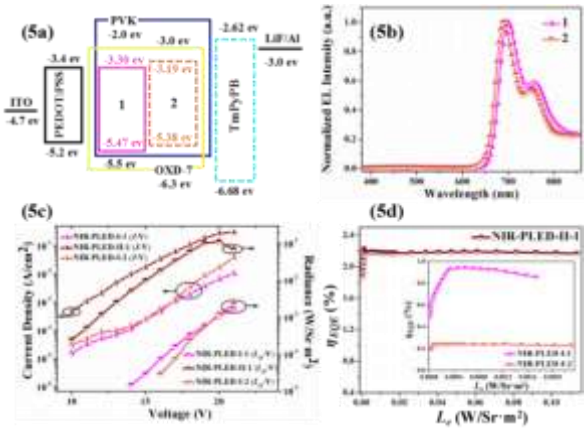

Figure 5. (5a) Device structures and energy level diagrams with TmPyPB or not; (5b) EL spectra; (5c) Current density (J, A/cm^2) and radiance (L_e, W/sr·m^2) as a function of applied voltage (V, v); (5d) η_{EQE} versus radiance (L_e) based on NIR-PLEDs I-II.

To further understand the electronic structures of the two NIR-emissive Ir(III)-complexes **1**-**2**, their electrochemical properties in anhydrous MeCN solution were investigated and frontier orbital energy levels were calculated, respectively, and the results were summarized in Table 1 and Figures 3-4. In the cyclic voltammograms shown in Figure 3, a reversible oxidation process is detected at half-wave potentials of +0.67 and +0.58 V versus Fc^+/Fc for complexes **1** and **2**, respectively, which should attributes to a predominantly metal-centered process also involving the cyclometalated benzo[*b*]thiophene moiety as evidenced by the following density functional theory (DFT) calculations (Figure 4). The relatively stronger anodic shift (0.09 V) in oxidation (HOMO level stabilization also in Figure 4) of complex **1** compared to complex **2**, probably ascribes to the stronger π-backbonding effect[17b] from the Ir(III)-center to the ancillary ligand for intra-molecular hydrogen-bonded complex **1** compared to BF_2-chelated complex **2**. In consideration of no distinctive reduction waving (also in Figure 3) for the two complexes and basis on the reasonable E_g^{OPT} value (2.17 eV of complex **1** versus 2.19 eV of complex **2**) in good accord with the slightly bathochromatic shift of complex **1** compared to **2**, the HOMO level at -5.47 eV or -5.38 eV and a LUMO level at -3.30 eV or -3.19 eV for complex **1** or **2** are calculated, respectively.

For a further insight into the photophysical and electrochemical characteristics of the two Ir(III)-complexes **1** and **2**, theoretic study of their electronic structures optimized at the ground state (S_0) in the gas state was carried out by DFT calculation. As shown in Figure 4, for both of complexes **1** and **2**, there has a similar density distribution of HOMO, where the HOMO dominates on the central Ir(III) ion and the benzo[*b*]thien-2-y groups of the two cyclometalated C^N (**iqbt**)$^-$ ligands and a small density distribution focuses on their isoquinoline rings. However, the LUMO concentrates on the central Ir(III) ion and one of the two cyclometalated C^N (**iqbt**)$^-$ ligands in complex **1**, while the other cyclometalated C^N (**iqbt**)$^-$ ligand and the (**hpa**)$^-$ moiety have no contribution to the LUMO. In contrast, the LUMO extends to the **BF_2-hpa** moiety in complex **2** with a spread density distribution. For comparison, although neither HOMO or LUMO has a direct contribution from the (**hpa**)$^-$ moiety for complex **1**, strong electronic perturbation assisted by its intra-molecular hydrogen bonding is approached, endowing the relatively higher Ir(III)-centered d-(t_{2g}) orbital HOMO and LUMO energies of -4.95 eV and -2.12 eV than those (-5.19 eV and -2.33 eV) of complex **2** with BF_2-chelated effect, correspondingly. In agreement with the E_g^{OPT}-sized trend, these DFT calculations also show a slightly narrower HOMO-LUMO gap of 2.83 eV for complex **1** than that (2.86 eV) of complex **2**.

Table 2 NIR performances of the NIR-PLEDs based on complexes **1**-**2**

Device	λ_{EL}^{max} (nm)	V_{on} (V)	η_{EQE}^{max} (%)	L_e^{max} (W/sr·m^2)
NIR-PLED-I-1	700, 760(sh)	19	0.94	1.7×10^{-3}
NIR-PLED-I-2	692, 752(sh)	18	0.24	2.3×10^{-3}
NIR-PLED-II-1	700, 760(sh)	11	2.22	0.11

Device performance of NIR-PLEDs based on the two Ir(III)-complexes 1-2

Thanks to the suitability of PVK-OXD7 with good hole-electron transport as the host,[17b] it is of special interest on using the efficient NIR-emitting complex **1** or **2** as the dopant for solution-processed NIR-PLEDs-I with a simple configuration shown in Figure 5(a). Attributing to the HOMO (-5.47 ~ -5.38 eV) and the LUMO (-3.30 ~ -3.19 eV) levels of complex **1** or **2** lie within the band gap (-6.3 ~ -5.5 eV of HOMO and -3.0 ~ -2.0 eV of LUMO) of PVK-OXD7, the injected electrons and holes through the PVK-OXD7 matrix are firstly trapped by the Ir(III)-complexes, and then direct charge trapping should occur within the NIR-emitting Ir(III)-complexes. Just as expected, as shown in Figure 5(b), the normalized EL spectra of the NIR-PLEDs-I exhibit voltage-independent while Ir(III)-complex-related NIR emissions resembling well those recorded for complexes **1**-**2** in solution (Figure 2), respectively. Apart from the strong peak at 700 nm along with a shoulder at 760 nm for NIR-PLED-I-**1** versus 692 nm along with 752 nm for NIR-PLED-I-**2**, their similar no observed fluorescence from the PVK-OXD7 host indicates that effective Förster energy transfer (addressing from the

significant spectra overlap between the emission of PVK with the absorption of complex **1** or **2** also shown in Figure 2)[24] from the host to the Ir(III)-complex-guest occurs during the charge-trapping process. For NIR-PLED-I-**1**, the turn-on voltage (V_{on}, defined as the voltage of 5×10^{-4} W/sr·m^2) is almost kept at 19 V, as shown in Figure 5(c), and in concomitance with the increase of the applied voltage (V), both the output irradiance (L_e) and the current density (J) monotonically increase to give the L_e^{max} of 1.7×10^{-3} W/sr·m^2 at 21 V with the J^{max} = 0.01 A/cm^2. Meanwhile, NIR-PLED-I-**1** exhibits the L_e-regulated waving for the η_{EQE} (Figure 5(d)), where the η_{EQE}^{max} of 0.94% is obtained and almost remains that constant (10% efficiency-roll-off) in the high L_e range of 0.2-1.8×10^{-3} W/sr·m^2. In contrast, due to slightly deeper trapping for complex **1** as compared to complex **2** with the same device configuration, NIR-PLED-I-**2** (also in Figure 5(c)) displays a lower V_{on} of 18 V while a higher L_e^{max} of 2.3×10^{-3} W/sr·m^2 at 21 V. Moreover, corresponding well with the lower Φ_{PL} of complex **2** in solution than that of complex **1**, the low η_{EQE}^{max} of 0.24% for NIR-PLED-I-**2** is shown with the L_e of 1.2×10^{-3} W/sr·m^2. Nonetheless, even upon the high irradiance with the L_e value up to 2.3×10^{-3} W/sr·m^2, down to 5% efficiency-roll-off (also in Figure (5d)) is observed for the NIR-PLED-I-**2**, which should be resulted from the significantly shorter radiative lifetime (τ = 0.76 μs) of complex **2** compared to complex **1** (τ = 2.13 μs).

In consideration of the distinctively higher EL efficiency while rather severe efficiency-roll-off (η_{EQE}^{max} = 0.94% and 10%) for NIR-PLED-I-**1** than those (η_{EQE}^{max} = 0.24% and 5%) of NIR-PLED-I-**2**, the trade-off balance between efficiency and efficiency-roll-off for NIR-PLED-I-**1** is conveniently realized from the electron-transporting promotion of Ir(III)-complex-emitters within. Toward the resolution to poor electron-trapping of Ir(III)-complex **1** arisen from the low energy level (-3.30 eV) of its LUMO, the supplement of TmPyPB facilitating electron-transport[25] is further considered. Through that structure optimization (also shown in Figure 5(a)) for NIR-PLED-II-**1**, more excitons are confined within the broadening recombination zone, and the increased carrier-trapping probability should be realized to exhibit an improved EL performance (also in Figures (5(b)-5(d)) as desired. Firstly, besides the Ir(III)-complex-**1** structural NIR emissions, the L_e^{max} up to 0.11 W/sr·m^2 and the illuminating voltage down to 11 V are observed. On the other hand, the η_{EQE}^{max} can be up to 2.22% for NIR-PLED-II-**1** with the L_e of 1.2×10^{-3} W/sr·m^2. Especially, the enhanced η_{EQE} values (2.18-2.22%) trade with almost negligible efficiency-roll-off (< 2%) during the whole illuminating process. Worthy of notice, the EL performances of the two NIR-PLEDs-I-II, especially NIR-PLED-II-**1** with effects of both intramolecular hydrogen bonded interaction and strengthened Föster energy transfer, are significantly superior to previously reported Ir(III)-complex-included solution-processed NIR-OLEDs[14] and comparable to the best of NIR-PLEDs.[15, 17b] Inspiringly, the simple post-modification (OH-based intramolecular hydrogen bond or BF_2-chelation) on pic-based ancillary ligand renders their [Ir(C^N)$_2$(L^X)]-complexes an opportunity to color and lifetime tunings within the NIR regime.

4. Conclusions

In summary, the hydroxyl group at the 3-position of pic ancillary ligand was introduced to induce two new [Ir(C^N)$_2$(L^X)]-characteristic complexes **[Ir(iqbt)$_2$(hpa)]** (**1**) with intramolecular hydrogen bond and **[Ir(iqbt)$_2$(BF$_2$-hpa)]** (**2**) with BF_2-chelation. That simple post-modification on the pic-based ancillary ligand can actually control the excited state of their [Ir(C^N)$_2$(L^X)] complexes for color and lifetime tunings. Moreover, based on the bathochromatic shift into the NIR regime for the two Ir(III)-complexes, efficient while weak efficiency-roll-off NIR-PLEDs are realized, where superior performance (η_{EQE}^{max} = 2.22% and almost negligible efficiency-roll-off) is exhibited for complex-**1**-doping NIR-PLED-II assisted by electron-transport TmPyPB. Importantly, that post-modification strategy to ancillary ligand for bathochromatic shift will offer a new approach to NIR-emissive Ir(III)-complexes for device applications.

Conflicts of interest

There are no conflicts to declare.

Acknowledgements

This work was funded by the National Natural Science Foundation (21373160, 91222201, 21173165), the Program for New Century Excellent Talents in University from the Ministry of Education of China (NCET-10-0936), the Doctoral Program (20116101110003) of Higher Education, the Science, Technology and Innovation Project (2012KTCQ01-37) of Shaanxi Province, the MOE Laboratory of Bioinorganic and Synthetic Chemistry, the Graduate Innovation and Creativity Fund (YZZ17127) and Wisteria Scientific Research Cooperation Special Project of Northwest University in P. R. of China and the National Science Foundation (1507871) in United States.

Notes and references

1 (a) C. Ulbricht, B. Beyer, C. Freibe, A. Winter and U. S. Schubert, *Adv. Mater.*, 2009, 21, 4418-4441; (b) W.-Y. Wong and C.-L. Ho, *Coord. Chem. Rev.*, 2009, 253, 1709-1758; (c) Q. Zhao, S. J. Liu and W. Huang, *Macromol. Rapid. Commun.*, 2010, 31, 794-807; (d) G. J. Zhou, W.-Y. Wong and X. L. Yang, *Chem. Asian J.*, 2011, 6, 1706-1727; (e) C.-L. Ho and W.-Y. Wong, *Coord. Chem. Rev.*, 2013, 257, 1614-1649; (f) X. B. Xu, X. L. Yang, J. Zhao, G. J. Zhou and W.-Y. Wong, *Asian J. Org. Chem.*, 2015, 4, 394-429; (g) U. Bin Mohd, R. Abd, A. J. Huckaba and M. K. Nazeeruddin, *Top. Curr. Chem.*, 2017, 375, 1-30; (h) Y. Chi, T.-K. Chang, P. Ganesan and P. Rajakannu, *Coord. Chem. Rev.*, 2017, 346, 91-100; (i) T. Y. Li, J. Wu, Z. G. Wu, Y. X. Zheng, J. L. Zuo and Y. Pan, *Coord. Chem. Rev.*, 2018, 374, 55-92.

2 (a) C. E. Housecroft and E. C. Constable, *Coord. Chem. Rev.*, 2017, 350, 155-177; (b) I. N. Mills, J. A. Porras and S. Bernhard, *Acc. Chem. Res.*, 2018, 51, 352-364.

3 (a) A. Volpe, A. Sartorel, C. Tubaro, L. Meneghini, M, Di Valentin, C. Graiff and M. Bonchio, *Eur. J. Inorg. Chem.*, 2014, 4, 665-675; (b) S. I. Bokarev, O. S. Bokareva and O. Kuehn, *Coord. Chem. Rev.*, 2015, 304-305, 133-145.

4 (a) V. Guerchais and J.-C. Fillaut, *Coord. Chem. Rev.*, 2011, 255, 2448-2457; (b) D.-L. Ma, S. Lin, W. H. Wang, C. Yang and C.-H. Leung, *Chem. Sci.*, 2017, 8, 878-889.

5 (a) K. K-W. Lo, *Acc. Chem. Res.*, 2015, 48, 2985-2995; (b) A. Zamora, G. Vigueras, V. Rodriguez, M. D. Santana and J. Ruiz, *Coord. Chem. Rev.*, 2018, 360, 34-76; (c) C. Caporale and M. Massi, *Coord. Chem. Rev.*, 2018, 363, 71-91; (d) T. C. Huang, Q. Yu, S. J. Liu, W. Huang and Q. Zhao, *Dalton Trans.*, 2018, 47, 7628-7633.

6 (a) G. J. Zhou, W.-Y. Wong and S. Suo, *J. Photochem. Photobio.,*

C, 2010, 11, 133-156; (b) C.-L. Ho and W.-Y. Wong, *New J. Chem.*, 2013, 37, 1665-1683; (c) X. L. Yang, G. J. Zhou and W.-Y. Wong, *Chem. Soc. Rev.*, 2015, 44, 8484-8575; (d) I. Omae, *Coord. Chem. Rev.*, 2016, 310, 154-169; (e) A. F. Henwood and E, Zysman-Colman, *Chem. Commun.*, 2017, 53, 807-826.

7 (a) C. Fan and C. L. Yang, *Chem. Soc. Rev.*, 2014, 43, 6439-6469; (b) L. Ying, C.-L. Ho, H. B. Wu, Y. Cao and W.-Y. Wong, *Adv. Mater.*, 2014, 26, 2459-2473; (c) X. L. Yang, G. J. Zhou and W.-Y. Wong, *J. Mater. Chem. C*, 2014, 2, 1760-1778.

8 (a) C.-L. Ho, B. Yao, B. H. Zhang, K.-L. Wong, W.-Y. Wong, Z. Y. Xie, L. X. Wang and Z. Y. Lin, *J. Organomet. Chem.*, 2013, 730, 144-155; (b) C. L. Ho, H. Li and W. Y. Wong, *J. Organomet. Chem.*, 2014, 751, 261-285.

9 J. Xue, C. Li, L. J. Xin, L. Duan and J. Qiao, *Chem. Sci.*, 2016, 7, 2885-2895.

10 (a) H. T. Whelan, R. L. Jr Smits, E. V. Buchman, N. T. Whelan, S. G. Turner, D. A. Margolis, V. Cevenini, H. Stinson, R. Ignatius and T. Martin, *J. Clin. Laser Med. Surg.*, 2001, 19, 305-314; (b) A. Rogalski and K. Chrzanowski, *Opto-Electron. Rev.*, 2002, 10, 111-136; (c) N. Tessler, V. Medvedev, M. Kazes, S. Kan and U. Banin, *Science*, 2002, 295, 1506-1508.; (d) D.-H. Kim, A. D'Aléo, X.-K. Chen, A. D. S. Sandanayaka, D. Yao, L. Zhao, T. Komino, E. Zaborova, G. Canard, Y. Tsuchiya, E. Choi, J. W. Wu, F. Frages, J.-L. Brédas, J.-C. Ribierre and C. Adachi, *Nat. Photonics*, 2018, 12, 98-104.

11 (a) R. Yang, R. Tian, J. Yan, Y. Zhang, J. Yang, Q. Hou and Y. Cao, *Macromolecules*, 2005, 38, 244-253; (b) S. V. Eliseeva and J.-C. G. Bünzli, *Chem. Soc. Rev.*, 2010, 39, 189-227; (c) G. Qian and Z. Y. Wang, *Chem. - Asian J.*, 2010, 5, 1006-1029; (d) H. F. Xiang, J. H. Cheng, X. F. Ma, X. G. Zhou and J. J. Chruma, *Chem. Soc. Rev.*, 2013, 42, 6128-6185; (e) F. C. J. M. van Veggel, *Chem. Mater.*, 2014, 26, 111-122.

12 K. T. Ly, R.-W. Chen-Cheng, H.-W. Lin, Y.-J. Shiau, S.-H. Liu, P.-T. Chou, C.-S. Tsao, Y.-C. Yang and Y. Chi, *Nat. Photonics*, 2017, 11, 63-68.

13 J. Xue, L. J. Xin, J. Y. Hou, L. Duan, R. J. Wang, Y. Wei and J. Qiao, *Chem. Mater.*, 2017, 29, 4775-4782.

14 (a) J. Qiao, L. Duan, L. T. Tang, L. He, L. D. Wang and Y. Qiu, *J. Mater. Chem.*, 2009, 19, 6573-6580; (b) R. Tao, J. Qiao, G. L. Zhang, L. Duan, C. Chen, L. D. Wang and Y. Qiu, *J. Mater. Chem. C*, 2013, 1, 6446-6454; (c) R. Tao, J. Qiao, G. L. Zhang, L. Duan, L. D. Wang and Y. Qiu, *J. Phys. Chem. C*, 2012, 116, 11658-11664; (d) L. J. Xin, J. Xue, G. T. Lei and J. Qiao, *RSC Adv.*, 2015, 5, 42354-42361; (e) Z. R. Hao, M. Lin, Y. J. Liu, Y. F. Wang, G. H. Xie and Y. Liu, *Dyes and Pigm*., 2018, 149, 315-322.

15 (a) E. L. Williams, J. Li and G. E. Jabbour, *Appl. Phys. Lett.*, 2006, 89, 083506-1-3; (b) X. S. Cao, J. S. Miao, M. R. Zhu, C. Zhong, C. L. Yang, H. B. Wu, J. G. Qin and Y. Cao, *Chem. Mater.*, 2015, 27, 96-104; (c) J. T. Yu, H. Tan, F, Y. Meng, K. Lv, W. G. Zhu and S. J. Su, *Dyes and Pigm.*, 2016, 131, 231-238; (d) Y. Liu, Z. R. Hao, F. Y. Meng, P. Wang, L. Yang, Y. F. Wang, Y. Pei and S. J. Su, *Chem. Phys. Lett.*, 2018, 699, 99-106.

16 (a) T. S. Qin, J. Q. Ding, B. Martin, L. X. Wang and K. Muellen, *Macromol. Rapid Commun.*, 2012, 33, 1036-1041; (b) M. Z. Chen, Y. Lan, J. Q. Zheng, F. F. Pang, X. Z. Song and L. He, *Dalton Trans.*, 2018, 47, 8023-8031.

17 (a) G. N. Li, Y. Zou, Y. D. Yang, J. Liang, F. Cui, T. Zheng, H. Xie and Z. G. Niu, *J. Fluoresc*, 2014, 24, 1545-1552; (b) S. Kesarkar, W. Mróz, M. Penconi, M. Pasini, S. Destri, M. Cazzaniga, D. Ceresoli, P. R. Mussini, C. Baldoli, U. Giovanella and A. Bossi, *Angew. Chem. Int. Ed.*, 2016, 55, 2714-2718.

18 I. Shigeru, Y. Shigeyuki, M. Takeshi, N. Hiroyuki, F. Hideki, K. Shiro and S. Yoshiaki, *Inorg. Chem. Commun.*, 2013, 38, 14-19.

19 A. B. Kajjam and S. Vaidyanathan, *Chem. Rec.*, 2018, 18, 293-349.

20 (a) T. Giridhar, W. Cho, Y.-H. Kim, T.-H. Han, T.-W. Lee and S.-H. Jin, *J. Mater. Chem. C*, 2014, 2, 9398-9405; (b) J. T. Yu, Y. F. Wang, Y. Liu, X. P. Deng, H. Tan, Z. Y. Zhang, M. X. Zhu and W. G. Zhu, *J. Organomet. Chem.*, 2014, 761, 51-55; (c) S. J. Yi, J.-H. Kim, Y.-J. Cho, J. W. Lee, T.-S. Choi, D. W. Cho, C. Pac, W.-T. Han, H.-H. Son and S. O. Kang, *Inorg. Chem.*, 2016, 55, 3324-3331; (d) Q. Zhang, Y. Y. Li, X. Wang, L. Wang and J. L. Zhang, *Mater. Chem. Phys.*, 2016, 177, 179-189; (e) X. L. Wang, H. Q. Yang, Y. P. Wen, L. Wang, J. F. Li and J. L. Zhang, *Inorg. Chem.*, 2017, 56, 8986-8995; (f) R. J. Davidson, Y.-T. Hsu, D. Yufit and A. Beeby, *Organometallics*, 2018, 37, 2003-2006.

21 H. B. Sun, L. J. Yang, H. R. Yang, S. J. Liu, W. J. Xu, X. M. Liu, Z. Z. Tu, H. Q. Su, Q. Zhao and W. Huang, *RSC Adv.*, 2013, 3, 8766-8776.

22 (a) A. D. Becke, *J. Chem. Phys.*, 1993, 98, 5648-5652; (b) C. Lee, W. Yangand R. G. Parr, Phys. Rev. B: Condens. *Matter Mater. Phys.*, 1988, 37,785-789.

23 M. J. Frisch, et al., *Gaussian 03*, Revision B.05, Gaussian, Inc.,Wallingford, CT, 2004.

24 (a) H. Y. Byun, I. J. Chung, H.-Y. Shim and C. Y. Kim, *Macromolecules*, 2004, 37, 6945-6953; (b) G. R. Fu, J. Q. Guan, B. N. Li, L. Liu, Y. N. He, C. Yu, Z. Zhang and X. Q. Lü, *J. Mater. Chem. C*, 2018, 6, 4114-4121.

25 (a) W-Y. Wong and C.-L. Ho, *J. Mater. Chem.*, 2009, 19, 4457-4482; (b) T. L. Ye, S. Y. Shao, J. S. Chen, L. X. Wang and D. G. Ma, *ACS Appl. Mater. Interfaces*, 2011, 3, 410-416; (c) T. Earmme and S. A. Henehke, *J. Mater. Chem.*, 2012, 22, 4660-4668.

Table of content

Elaborated from the effect of intramolecular hydrogen bond or BF_2-chelation, two new heteroleptic iridium(III)-complexes **1**-**2** capable of NIR-emitting are used to fabricate NIR-PLEDs, where especially through complex-**1**-doping, high efficiency (η_{EQE}^{max} = 2.22%) and almost negligible efficiency-roll-off are realized.